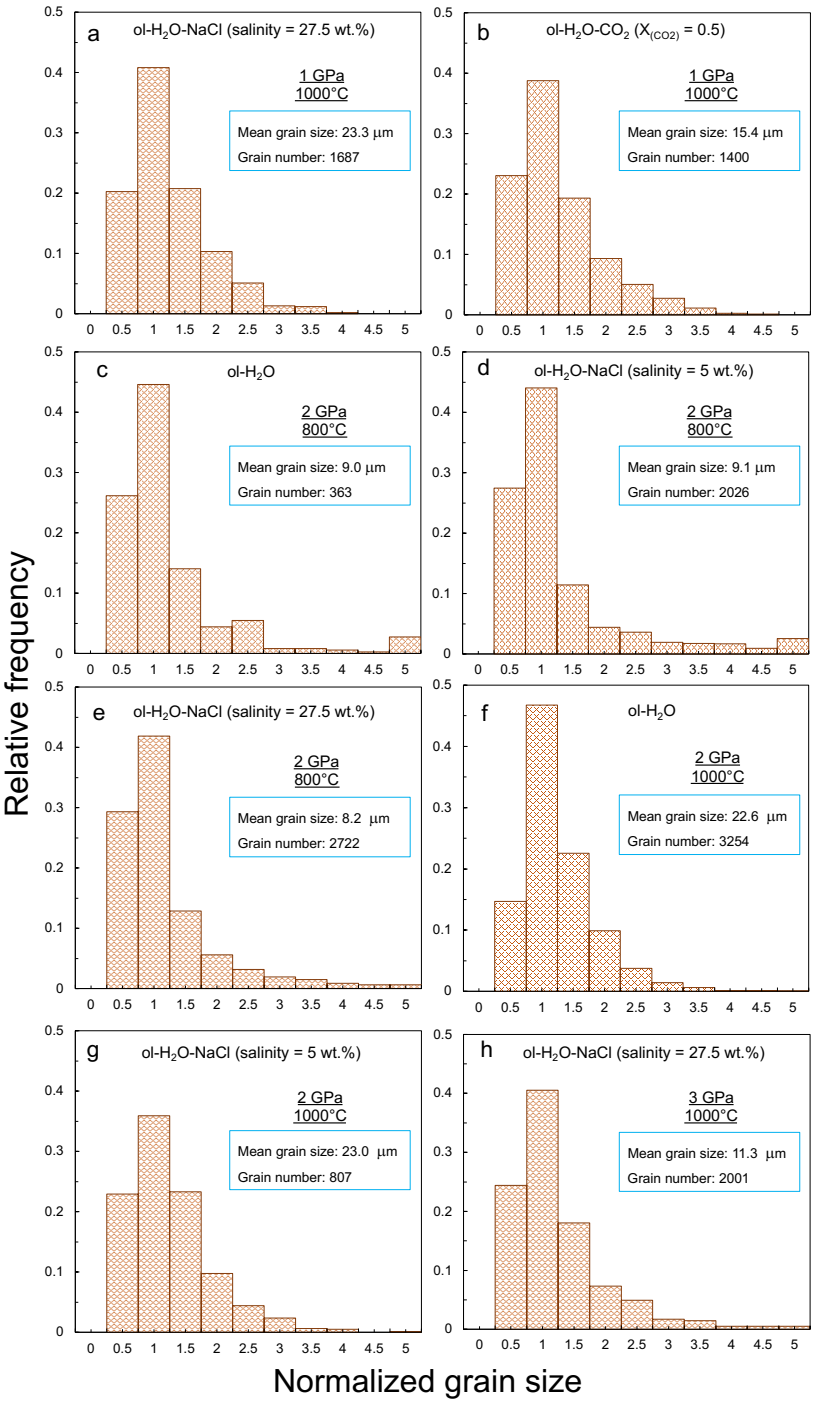

FIGURE S1. Histogram of normalized grain size distribution in the olivine–fluid system. The grain size distribution was normalized by the mean grain size of the recovered sample. The grain size peak is concentrated around the mean grain size. The mean grain size and measured grain number are shown in the panel. Abbreviation: ol = olivine.

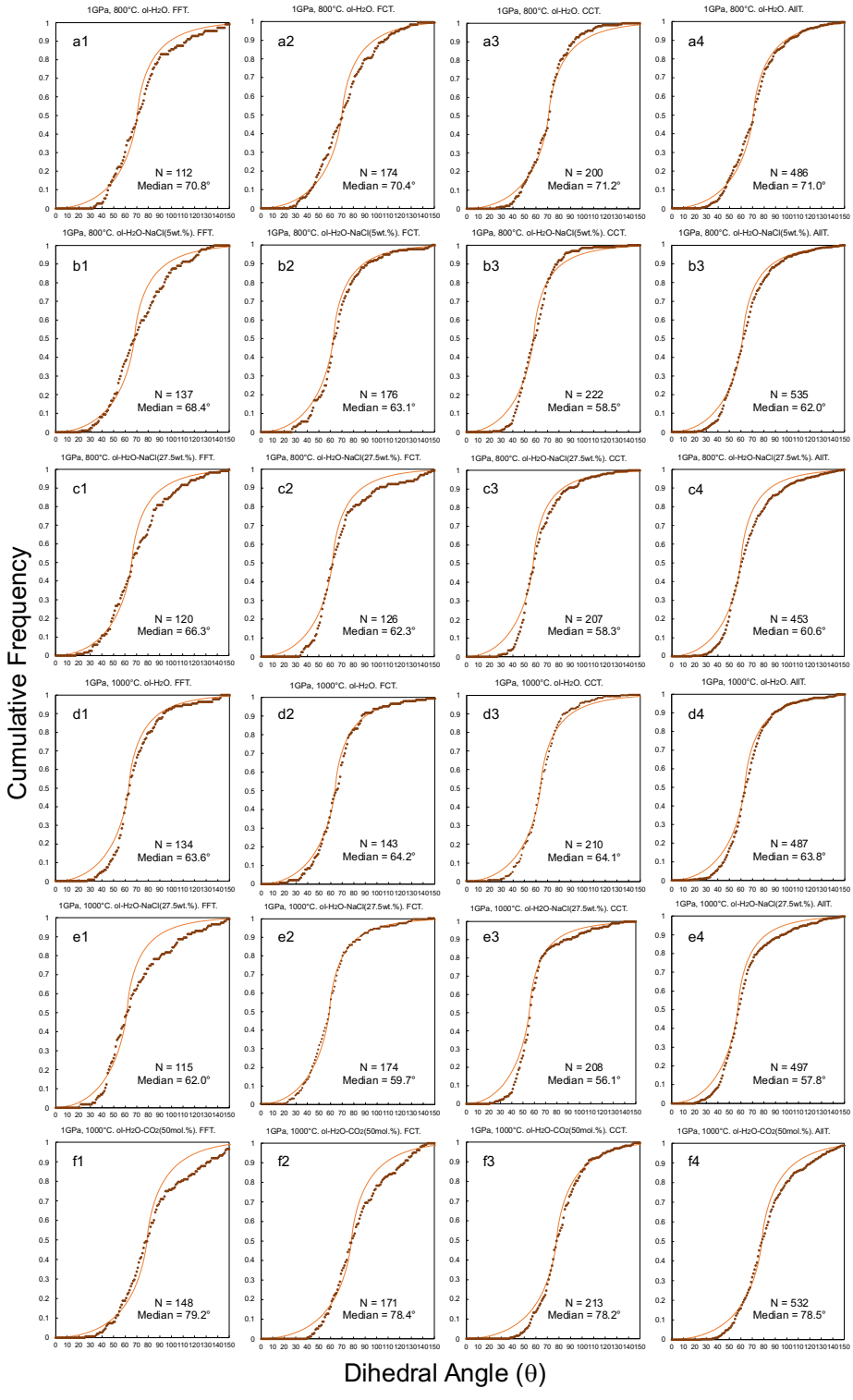

FIGURE S2. Cumulative frequency curves of measured apparent dihedral angles (θ) in olivine–fluid systems at 1–3 GPa and 800–1100 °C. The median value and number (N) of the measured angles are shown for each experimental condition. The solid lines represent the theoretical cumulative frequency curves of the isotropic system with one true θ (Jurewicz and Jurewicz 1986). This angle is assumed to coincide with the obtained median value. P–T conditions and fluid composition are shown for each system. Abbreviations: ol = olivine, FFT = faceted–faceted angle, FCT = faceted–curved angle, CCT = curved–curved angle, AllT = all types of measured angle.

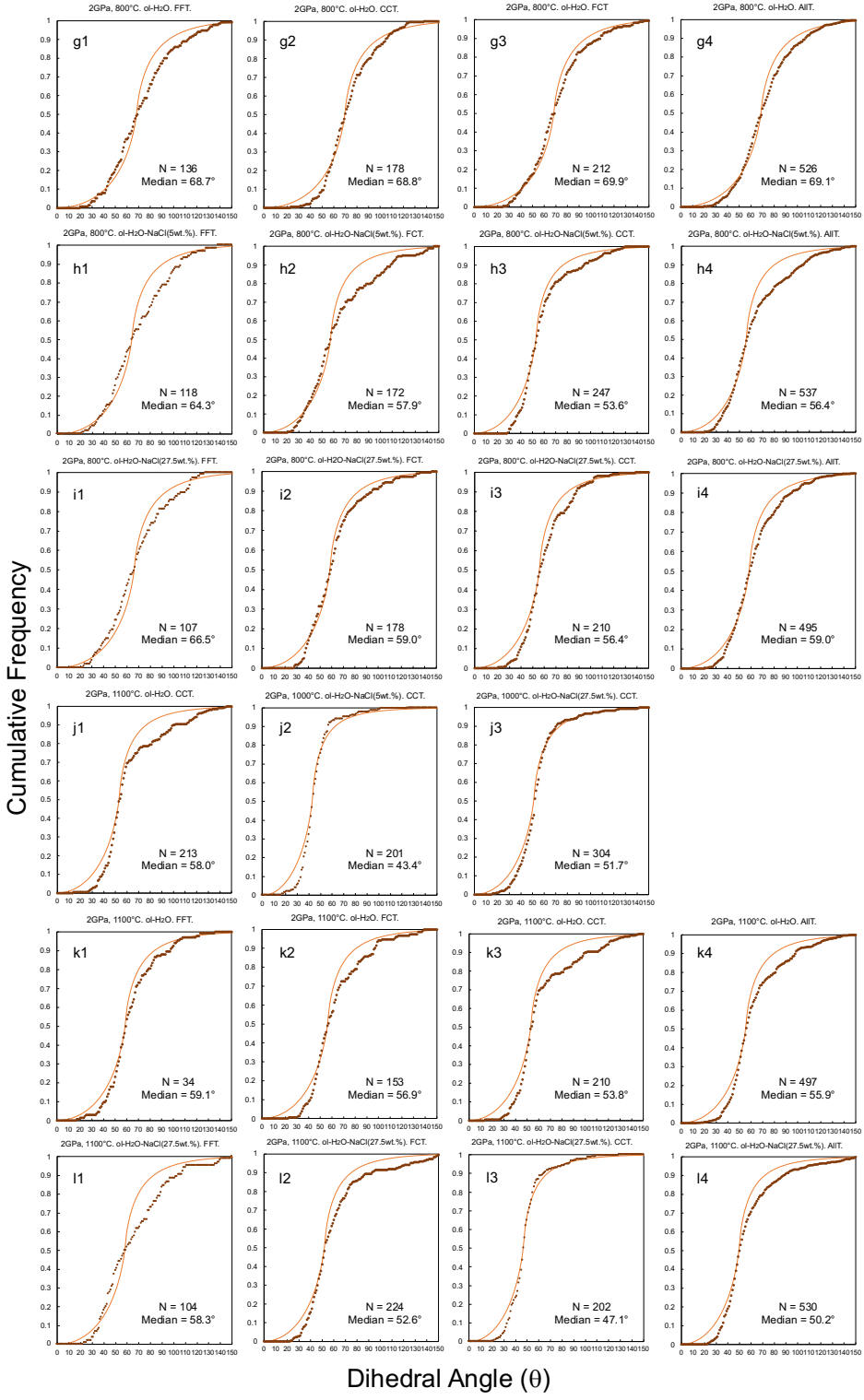

FIGURE S2.—*CONTINUED*

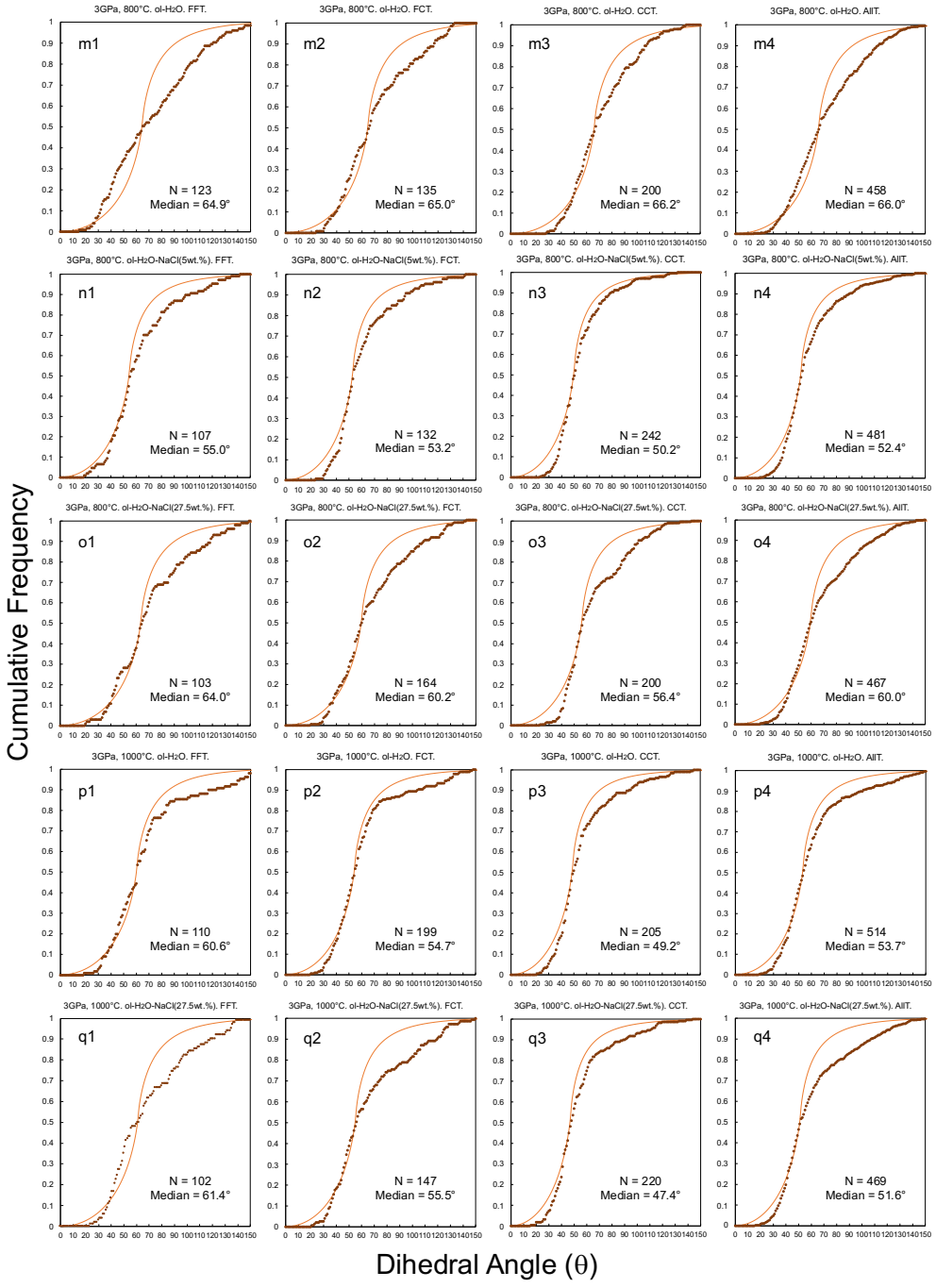

FIGURE S2.—*CONTINUED*

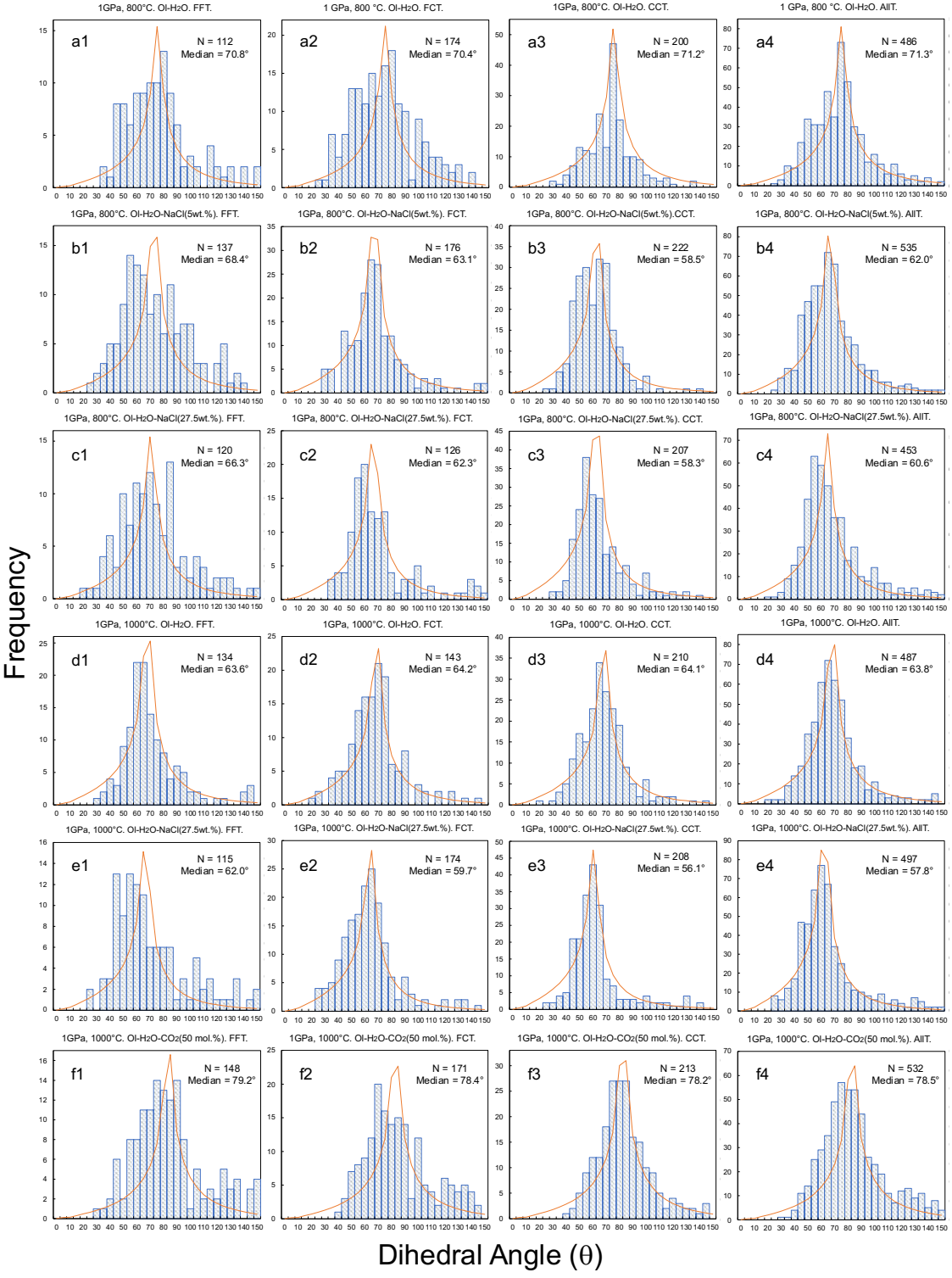

FIGURE S3. Frequency distribution histograms of measured apparent dihedral angles (θ) in olivine–fluid systems at 1–3 GPa and 800–1100 °C. Theoretical distributions (orange curves) for mono–mineral and isotropic systems are also shown in the histograms along with the median values (Jurewicz and Jurewicz 1986). The P–T and fluid composition are shown for each system. Abbreviations: ol = olivine, FFT = faceted–faceted angle, FCT = faceted–curved angle, CCT = curved–curved angle, AllT = all types of measured angle.

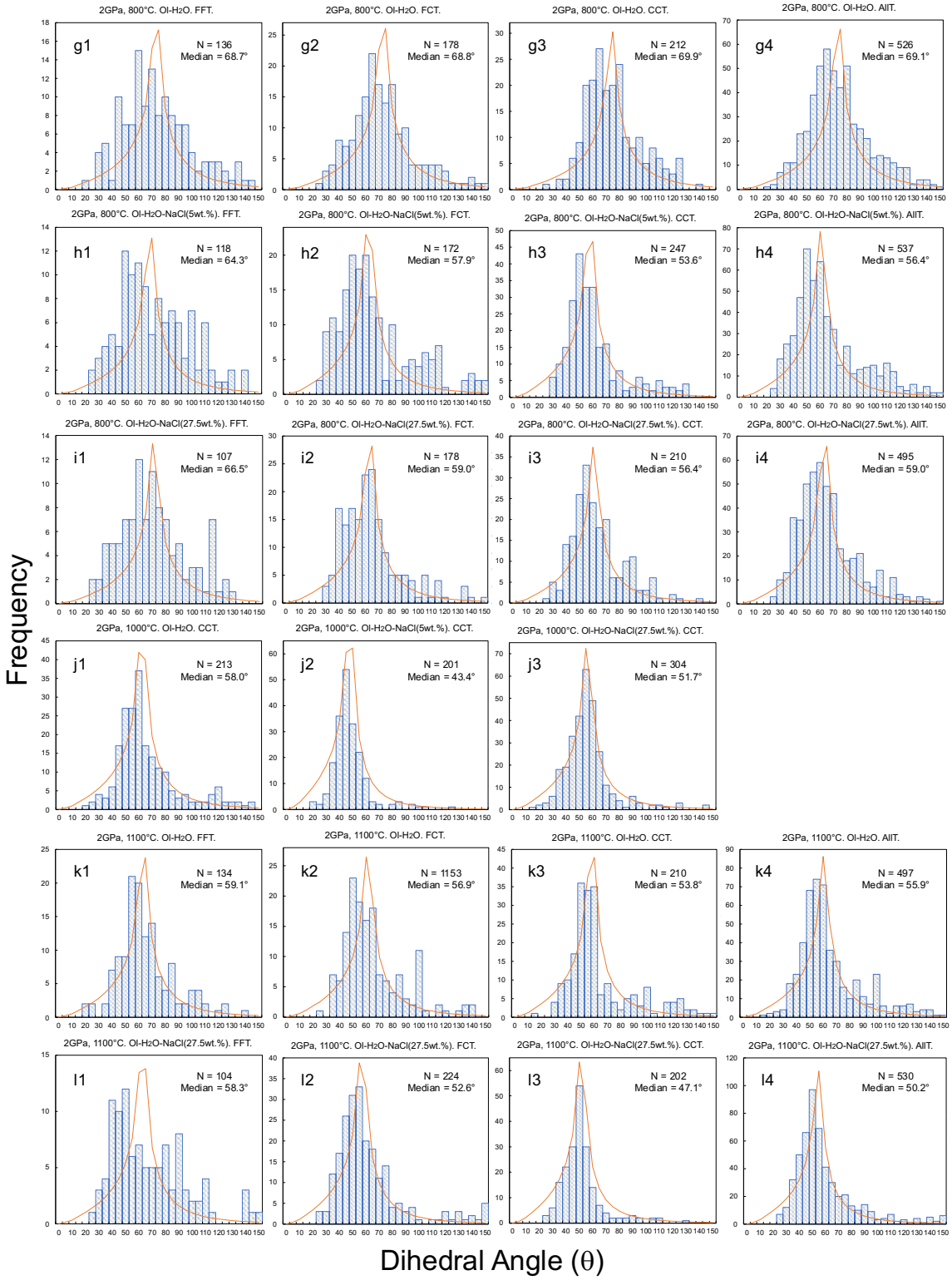

FIGURE S3.—*CONTINUED*

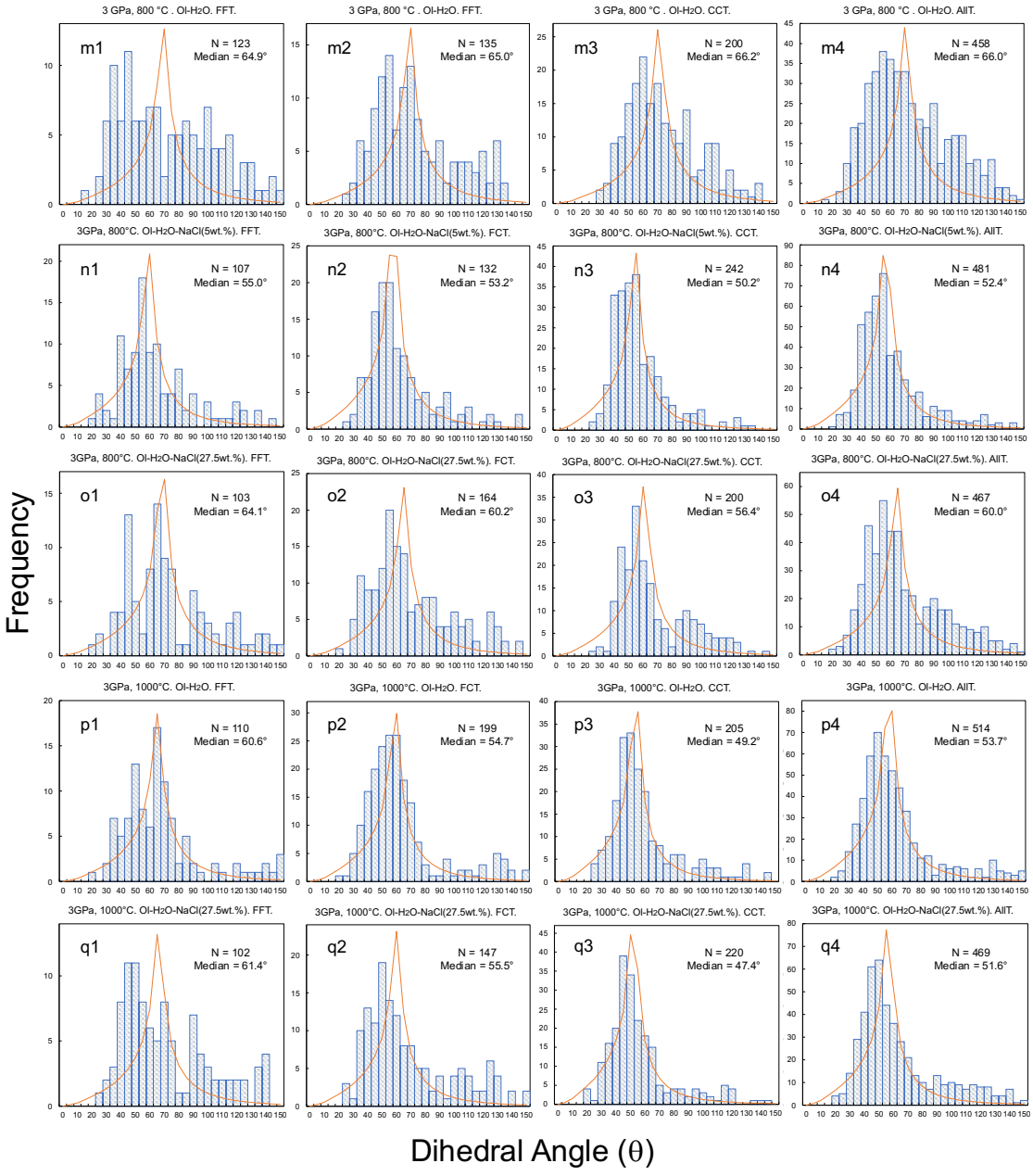

FIGURE S3.—*CONTINUED*

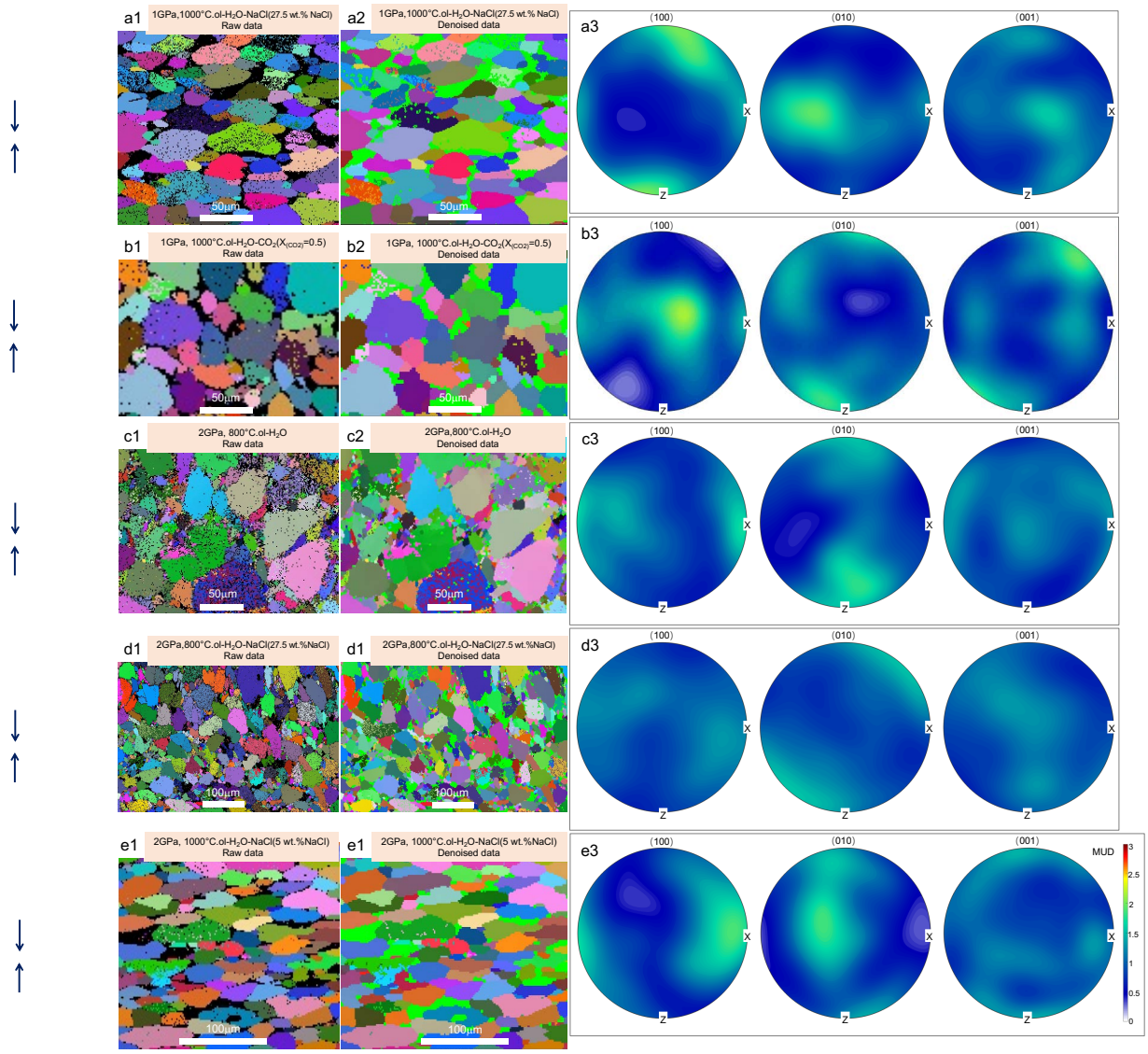

FIGURE S4. EBSD maps and corresponding pole figures under static compression conditions. **a1–e1** Raw EBSD maps of recovered olivine aggregate in olivine–fluid systems. Small points within grains are attributed to noise, crystal defects, and fluid inclusions. **a2–e2** Denoised EBSD maps corresponding to **a1–e1**. Points smaller than 1 μm have been removed. All grains defined by different colors are olivine with different orientations. **a3–e3** Pole figures showing the crystallographic orientation of (100), (010), and (001) corresponding to **a2–e2**. Color intensities are multiples of the random distribution (MUD). *P–T* conditions and fluid composition are shown along with the corresponding system. Abbreviation: ol = olivine.

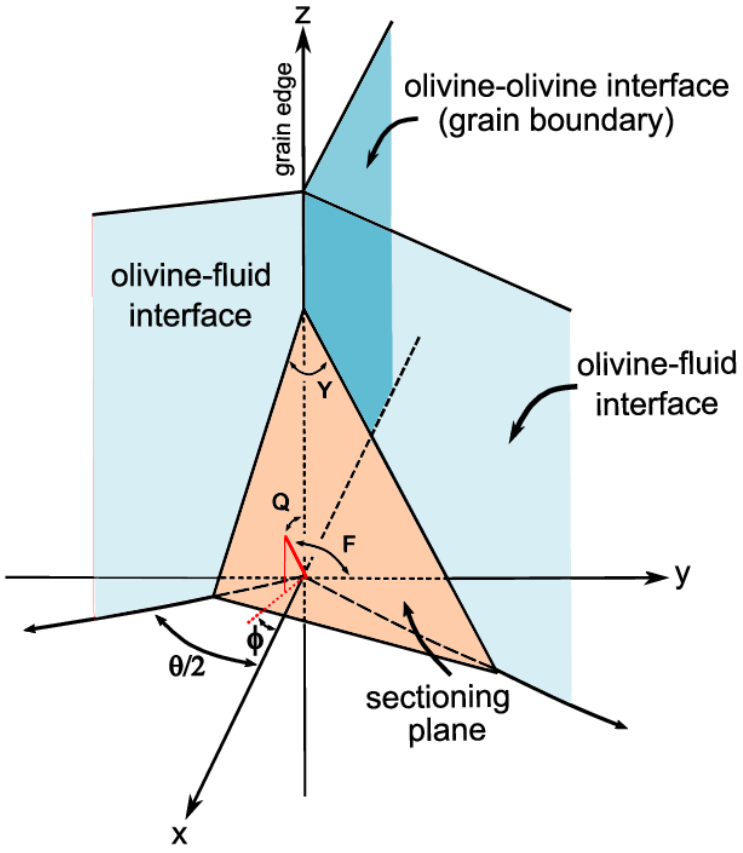

FIGURE S5. Schematic olivine–olivine–fluid triple junction with a sectioning plane after Harker and Parker (1945) and Jurewicz and Jurewicz (1986). True dihedral angle (θ) formed by two olivine–fluid interfaces (pale blue planes). Y is the apparent dihedral angle observed on the sectioning plane (pale orange plane). The bold red line represents the unit normal of the sectioning plane defined in the angular coordinates Q and ϕ. F is the angle formed by the sectioning plane and grain boundary plane (deep sky blue plane).

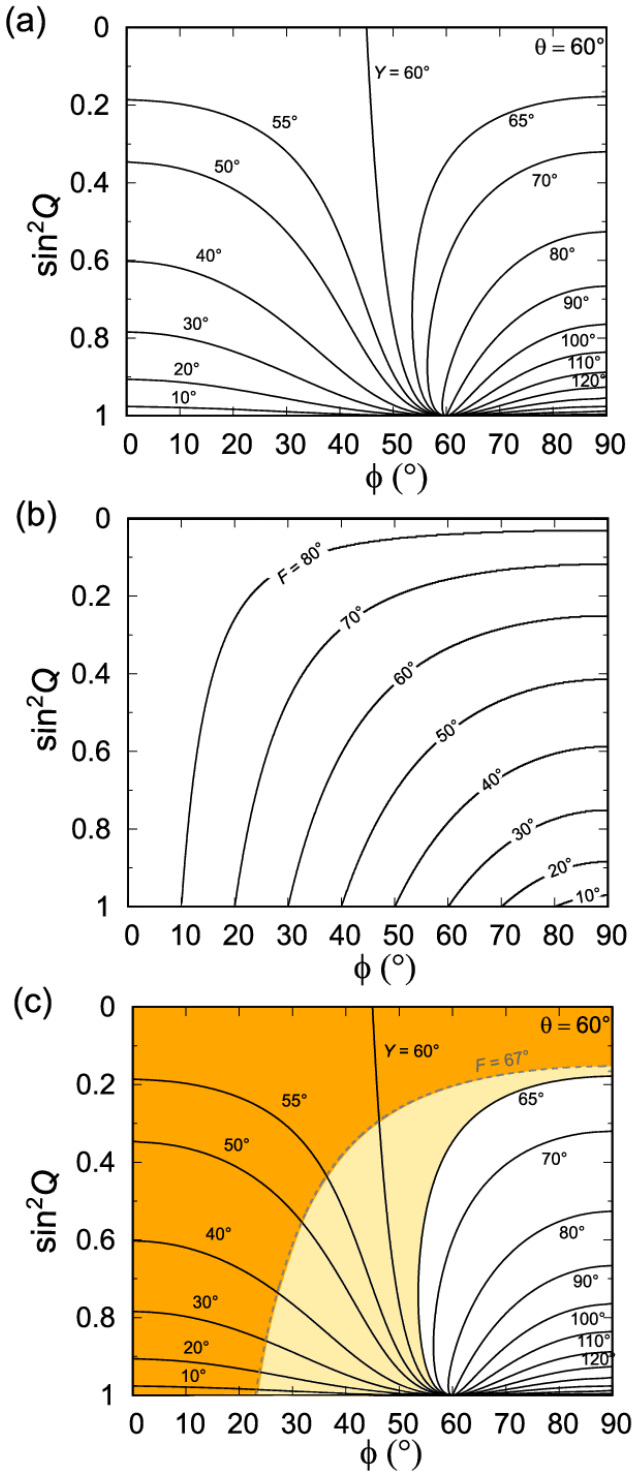

FIGURE S6. Sectioning calculation at the olivine–olivine–fluid triple junction. (**a**) Contours of the apparent dihedral angle, Y in the $\sin^2 Q$ vs. ϕ diagram calculated according to Harker and Parker (1945) assuming a true dihedral angle, θ of 60°. (**b**) Contours of the angle formed by the grain boundary plane and sectioning plane, F, in the $\sin^2 Q$ vs. ϕ diagram. (**c**) Area of $F \geq 67°$ within the Y window of 0–65° in the $\sin^2 Q$ vs. ϕ diagram (orange). The ratio of this area to the area of Y = 0–60° (orange + pale yellow) yields the probability of $F \geq 67°$ in the selected Y window.

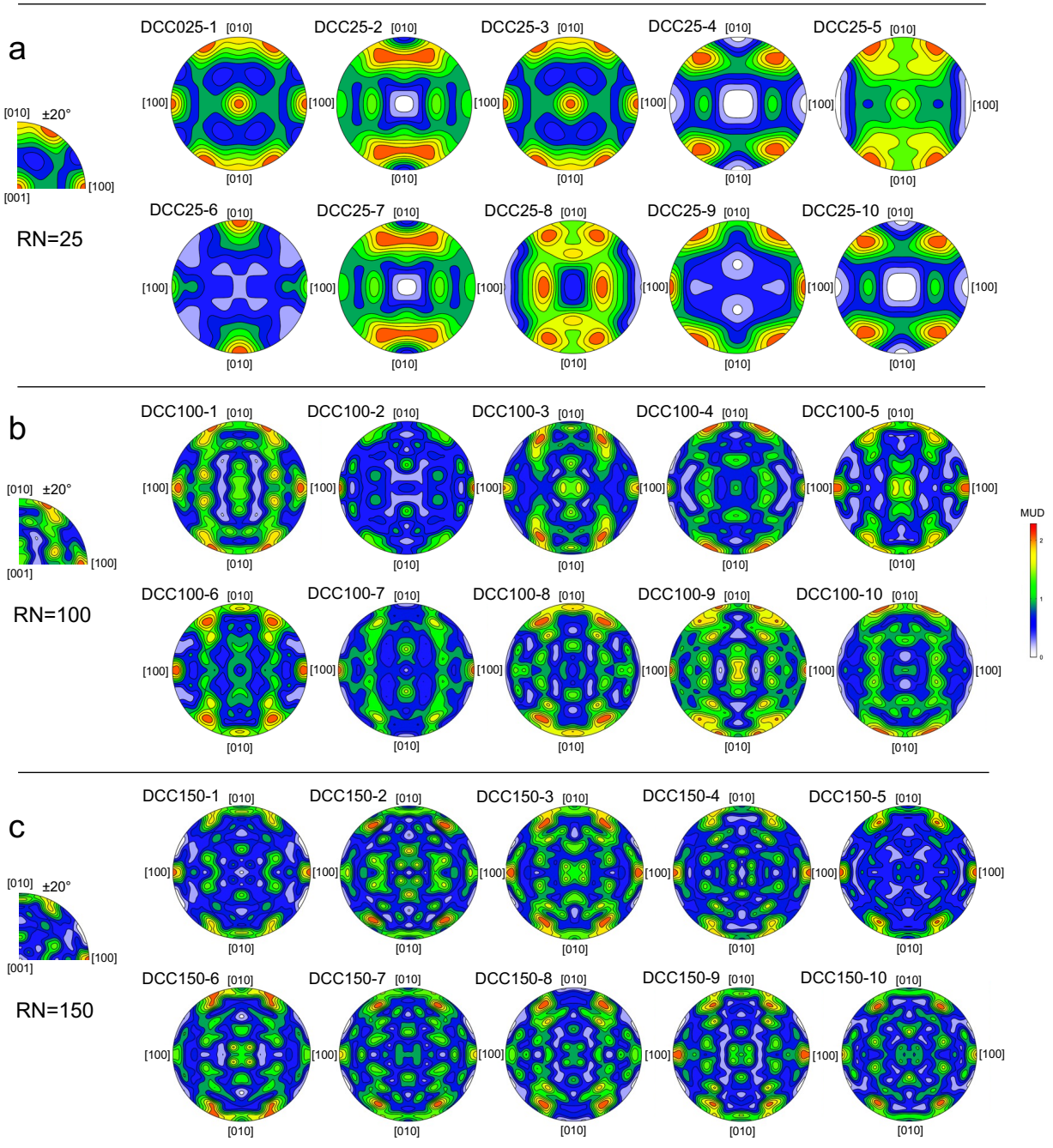

FIGURE S7. Random test of the DCC dataset (b3 in Figure 8). (**a**) Test repeated 10 times with 25 randomly selected measurements. (**b**) Test repeated 10 times with 100 randomly selected measurements. (**c**) Test repeated 10 times with 150 randomly selected measurements. The number of random selections (RN) is shown for each series of tests. The scale is in units of multiples of uniform distribution (MUD). The assumed error is ±20°.